Effect of Direct Recycling Hot Press Forging Parameters on Mechanical Properties and Surface Integrity of AA7075 Aluminum Alloys

Ruhaizat, Nasha Emieza; Yusuf, Nur Kamilah; Lajis, Mohd Amri; Al-Alimi, Sami; Shamsudin, Shazarel; Tukiat, Ikhwan Shah Tisadi

DOI:
10.3390/met12101555

Publication date:
2022

metals

MDPI

Article

Effect of Direct Recycling Hot Press Forging Parameters on Mechanical Properties and Surface Integrity of AA7075 Aluminum Alloys

Nasha Emieza Ruhaizat [1], Nur Kamilah Yusuf [1,*], Mohd Amri Lajis [1], Sami Al-Alimi [1], Shazarel Shamsudin [1], Ikhwan Shah Tisadi Tukiat [1] and Wenbin Zhou [2]

[1] Sustainable Manufacturing and Recycling Technology, Advanced Manufacturing and Materials Center (SMART-AMMC), Universiti Tun Hussein Onn Malaysia (UTHM), Parit Raja 86400, Malaysia
[2] Department of Mechanical Engineering, Imperial College London, London SW7 2AZ, UK
* Correspondence: nurkamilah@uthm.edu.my; Tel.: +60-7-4537325

Abstract: The current practice in aluminum recycling plants is to change the waste into molten metal through the conventional recycling (CR) manufacturing process. However, the CR technique is so energy-intensive that it also poses an indirect threat to the environment. This paper presents a study on meltless direct recycling hot press forging (DR-HPF) as an alternative sustainable approach that has fewer steps with low energy consumption, as well as preventing the generation of new waste. A laboratory experiment was conducted to study the mechanical properties and surface integrity of AA7075 aluminum alloy by employing a hot press forging (HPF) process under different temperatures (380, 430, and 480 °C) and holding times (0, 60, and 120 min). It was found that as the parameter increased, there was a positive increase in ultimate tensile strength (UTS), elongation to failure (ETF), density, and microhardness. The recycled chips exhibit the best mechanical properties at the highest parameters (480 °C and 120 min), whereas the UTS = 245.62 MPa and ETF = 6.91%, while surface integrity shows that the calculated microhardness and density are 69.02 HV and 2.795 g/cm^3, respectively. The UTS result shows that the highest parameters of 480 °C and 120 min are comparable with the Aerospace Specification Metals (ASM) Aluminum AA7075-O standard. This study is a guide for machinists and the manufacturing industry to increase industry sustainability, to preserve the earth for future generations.

Keywords: direct recycling; hot press forging (HPF); solid-state recycling (SSR); AA7075 aluminum alloy; mechanical properties; surface integrity

Citation: Ruhaizat, N.E.; Yusuf, N.K.; Lajis, M.A.; Al-Alimi, S.; Shamsudin, S.; Tukiat, I.S.T.; Zhou, W. Effect of Direct Recycling Hot Press Forging Parameters on Mechanical Properties and Surface Integrity of AA7075 Aluminum Alloys. *Metals* **2022**, *12*, 1555. https://doi.org/10.3390/met12101555

Academic Editor: Koh-ichi Sugimoto

Received: 29 August 2022
Accepted: 17 September 2022
Published: 20 September 2022

1. Introduction

Raw material production consumes roughly 21% of the world's energy demand and accounts for 25% of global carbon dioxide emissions [1,2]. The second most produced metal after steel is aluminum, which is also the most commonly produced non-ferrous metal [3]. As far as lightweight metal is concerned, from 2005 to 2050, aluminum demand is predicted to increase by a factor of 2.6–3.5 [4,5]. Aluminum alloys have become quite popular in the automotive and aerospace industry, due to their excellent properties [6–8]. AA7075 is a group of AlZnMgCu or 7xxx series aluminum alloys that are used to manufacture aircraft and aerospace vehicles, where a combination of high strength, hardness, and corrosion resistance are required [9–11]. The continuous increase in aluminum consumption has led to a rise in the quantity of aluminum scrap [12].

The production of raw aluminum alloys from bauxite ore requires a huge amount of energy consumption [13,14]. To minimize anthropogenic carbon dioxide emissions and decouple economic growth from resource use, it is necessary to reduce raw material demand. [15]. Aluminum recycling is implemented as a countermeasure. The most notable benefit of aluminum recycling is its ability to significantly reduce the extraction of

virgin ores, protect non-renewable resources, and minimize the devastation of the landscape [16,17]. Aluminum recycling is more cost-effective compared to other materials and the alloy properties are not adversely affected by the recycling process [18]. Moreover, aluminum recycling can reduce carbon dioxide emissions by 93% [19]. Several studies have addressed that aluminum recycling requires only 5% of the energy required for raw metal production, implying that it represents a significant opportunity to reduce environmental risk if managed sustainably [20,21]. Despite these gains, there is still room to make the recycling process more efficient and less resource-intensive.

Conventional recycling (CR) is a current remelting-based practice used in most recycling plants, which involves charging scrap into a molten state [22]. As far as lightweight aluminum alloys are concerned, the CR approach is still energy-intensive and demonstrates low energy efficiency [23,24]. In every remelting process, metal losses occur in slag mixing and metal oxidation [25,26]. By replacing metal permanent losses with primary aluminum, the embodied energy of recycled aluminum can increase by up to 30 megajoules/kg [15,27]. The disposal of hazardous dross has been a concern for the aluminum industry [28]. In a recent study, Hatayama et al. forecasted that 6.1 megatons of aluminum scrap would be unable to be recycled by 2030 due to concentrated alloying elements [29]. Since the removal of alloying elements during the remelting process is difficult in the case of most of the elements, hence, a different approach focusing on solid-state recycling (SSR) can offer significant environmental benefits by preventing aluminum loss during remelting [30]. The method of direct SSR promises a significant energy reduction compared to the CR technique, which requires a very high temperature to reach the melting point [31,32]. A review paper written by Wan et al. clustered the SSR process into two sub-categories, namely, powder metallurgy (PM) and severe plastic deformation (SPD) [16]. For plastic deformation to be effective, it should be sufficient to fracture the surface oxide layer that hinders metallic bonding [33]. To date, various SPD processes have been studied, including cold extrusion, hot extrusion, compaction, forging, friction extrusion, sideways extrusion, and compressive torsion [34–39].

Initially, the SSR technique utilizes the powder metallurgy processes developed by Gronostajski et al. [40], as followed up in studies conducted by Fogagnolo et al. [41]. Some of the SSR techniques that have been studied lead to bestowing excellent mechanical properties by employing powder metallurgy and extrusion processes [42–48]. Meanwhile, in a recent work, Al-Alimi et al. successfully employed hot extrusion, followed by a hot equal-channel angular processing (ECAP) process [49]. According to the findings, further plastic deformation by hot ECAP following hot extrusion greatly improved the mechanical properties of recycled aluminum, compared to samples obtained solely from hot extrusion [49–51]. Khajouei-Nezhad et al. examined the properties of recycled aluminum composite, using a high-pressure torsion (HPT) process [52]. The study concluded that the addition of aluminum powder as a binder enhanced the mechanical performance, which reduced porosity and improved metallic bonding. According to the research published by Kuzman et al., smaller and simpler chips provided better input material for cold compression [53]. Khamis et al. investigated the direct hot press forging (HPF) process and discovered that the most influential factor on mechanical strength was holding time, followed by pre-compaction and aluminum chip size [54]. The HPF technique is a single-step process that has garnered interest and will be pursued further in this study.

The present paper will be employing the direct recycling hot press forging (DR-HPF) process as an alternative sustainable approach. The deformation of the HPF process occurs at a temperature above the metal recrystallization temperature [55]. This fewer-step approach is known as direct recycling by eliminating the pre-processing steps of cold-compaction and ball milling, thus reducing the cost, time, and energy consumption [55–57]. The purpose of this paper is to explore the potential of the HPF process, to be used for manufacturing AA7075 aluminum chips as secondary products. Many researchers agree that temperature is the most important factor to consider when dealing with aluminum alloys [32,47,58]. To validate this, a study on the effect of DR-HPF parameter setting on the

mechanical properties and surface integrity will be presented in this study. The parameter setting for the HPF process is crucial for improving the mechanical properties and surface integrity of recycled AA7075 aluminum billets.

2. Materials and Methods

This section briefly elaborates on a general plan of experimental work. This study focuses on the recycling of AA7075 aluminum chips using hot press forging (HPF) at different process parameters of operating temperature and holding time. Several tests on the material's mechanical properties and surface integrity were conducted to observe the potential of the recycling process by improving the quality of the recycled specimen. The analysis of mechanical properties included ultimate tensile strength (UTS) and elongation to failure (ETF). Meanwhile, the analysis of surface integrity included the testing of microstructure, grain analysis, fracture, density, and microhardness.

2.1. Material Preparation and Processing

The chemical element of the AA7075 bulk material is depicted in Table 1. It was measured via energy-dispersive X-ray spectroscopy (EDS) using a field-emission scanning electron microscope (FESEM), brand JSM-7600F, JEOL, Akishima, Japan. Aluminum alloy is the main element of AA7075 alloys (87.1–91.4 wt %). It has been proven that the material used in this study is AA7075 aerospace alloy, by comparing it to the percentage of elements found in the ASM material data sheet.

Table 1. The element composition of the as-received AA7075 aluminum matrix.

Elements	Weight Percentage (wt %)
Aluminum, Al	88.21
Magnesium, Mg	3.01
Silicone, Si	0.25
Titanium, Ti	0.18
Chromium, Cr	0.26
Iron, Fe	0.39
Copper, Cu	1.61
Zinc, Zn	6.08

The commercial AA7075 aluminum bulk was milled using high-speed machining (Mazak NEXUS 410A-II, Oguchi, Japan) to produce aluminum chips. The produced chips were cleaned in acetone solution for 10 min using an ultrasonic bath (Elmasonic S 60 H, Elma, Wetzikon, Switzerland) and then dried for 30 min in a thermal oven (SOV140B, KWF, Beijing, China) at 60 °C. The standard practice for cleaning and drying follows ASTM G131-96 and the procedure used by Yusuf (2017) [59]. The chips must not contain any contaminants or impurities that would affect their chemical composition and impede the diffusion of metal chip bonding throughout the manufacturing process.

The cleaned AA7075 chips were filled and compacted into a dog-bone closed die. The aluminum recycling process was performed using a laboratory hot press forging (HPF) machine, UTHM, Malaysia. The hot press forging (HPF) process, as shown in Figure 1, was executed at a constant pressure of 35 tonnes, with a four-times pre-compacting cycle. Figure 2 portrays the process diagram of DR-HPF. The selected operating temperatures in this process are 380, 430, and 480 °C, and the holding times are 0, 60, and 120 min. The recommended range of forging temperatures for AA7075, based on the ASM handbook committee, volume 14A is between 380 and 440 °C [60]. However, Yusuf et al. (2013) suggested that the forging temperature must be chosen to fall between the solidus and recrystallization temperatures [58]. It has been proposed that the recrystallization temperature for AA7075 should be between 430 and 480 °C [61], while the solidus temperature started at 477 °C (ASM Material Data Sheet). Meanwhile, the most commonly selected holding time from the previous studies for AA7075 is 60 min [62–67]. As a result, the

temperature and holding time chosen in this study are based on the previously indicated recommended data. Recycled specimens with different parameter settings are presented in Table 2. The recycled samples after the DR-HPF process are denoted as T1- temper and will be compared with theoretical ASM AA7075-O, to observe the potential properties of the secondary material.

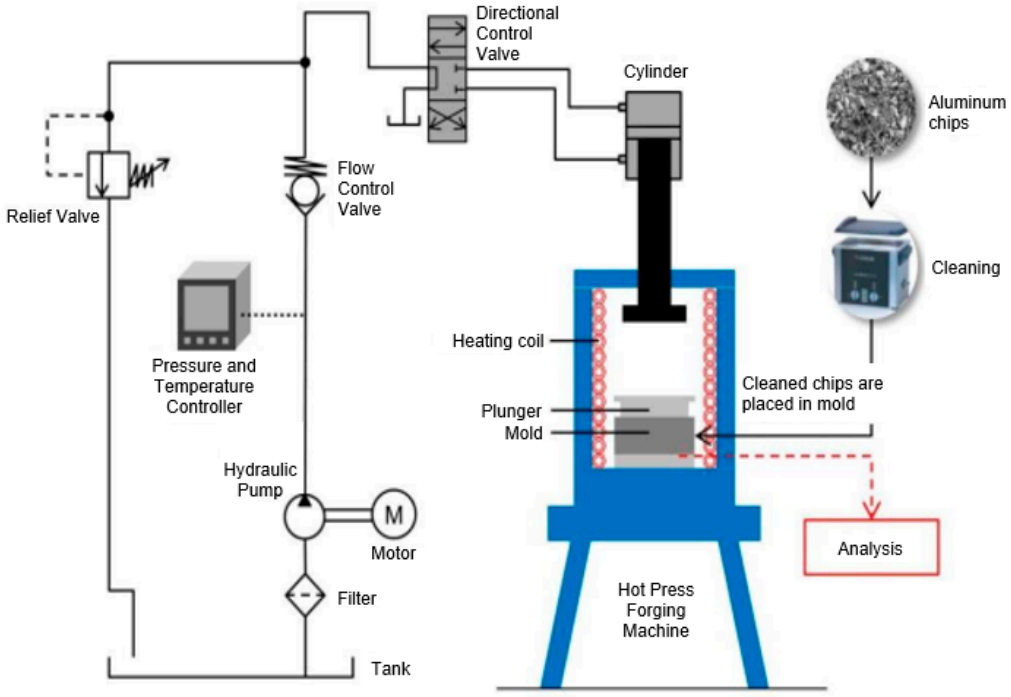

Figure 1. Experimental set-up of the hot press forging (HPF) process [68].

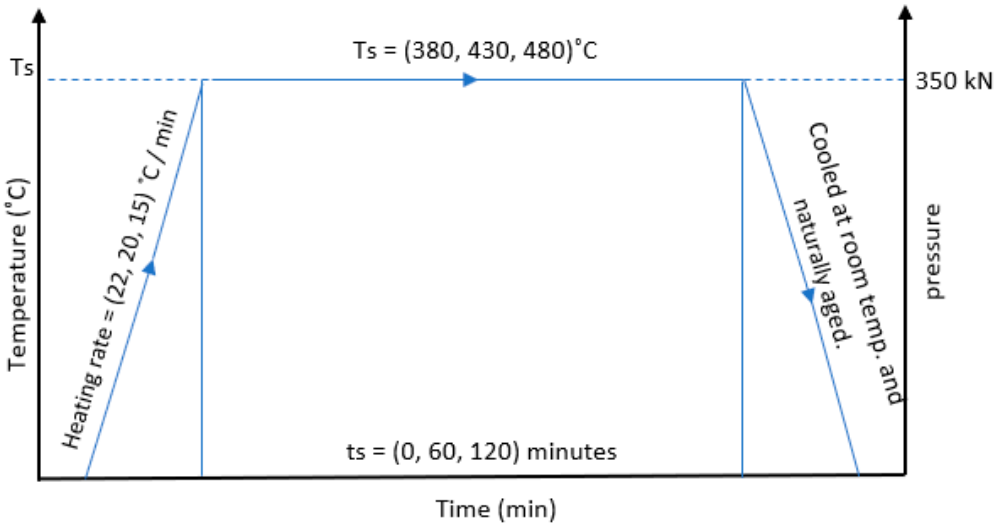

Figure 2. The HPF process diagram.

2.2. Mechanical Characterization

Tensile tests were carried out at room temperature using a universal testing machine (UTM), the Shimadzu Servopulser, Kyoto, Japan, EHF-EM0100K1-020-0A, with a 25 kN load and a gauge length of 25 mm to record the strain. The tests were performed at a speed of 1 mm/min. The detailed dimensions of the dog-bone recycled specimens with standard size specifications are shown in Figure 3 and Table 3.

Table 2. The HPF process parameter for operating temperature and holding time.

Sample Designation	Operating Temperature, Ts (°C)	Holding Time, ts (min)
S1	380	0
S2	380	60
S3	380	120
S4	430	0
S5	430	60
S6	430	120
S7	480	0
S8	480	60
S9	480	120

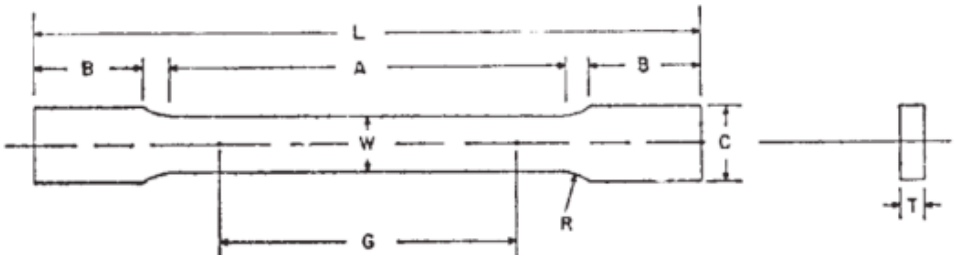

Figure 3. The dimension of recycled specimens for the tensile test (ASTM E8/E8M-16a).

Table 3. The standard size specifications for dog-bone recycled specimens.

Subsize Sample (6 mm Wide)	Dimensional (mm)
G—Gauge length	25
W—Width	6
T—Thickness	<6
R—Radius of fillet, min	6
L—Overall length, min	100
A—Length of reduced section, min	32
B—Length of grip section, min	30
C—Width of grip section, approximate	10

Based on in Figure 3, A refers to the length of the reduced section which is 32 mm, B refers to the length of the grip section which is 30 mm, C refers to the approximate width of the grip section which is 10 mm, L refers to the overall length which is 100 mm, W refers to the width which is 6 mm, G refers to the gauge length which is 25 mm, T refers to the thickness which is less than 6 mm and R refers to the radius of the fillet which is 6 mm.

2.3. Surface Integrity

2.3.1. Microstructure Analysis

A SU1510 scanning electron microscope (SEM) (Hitachi, Ibaraki, Japan) was used to study the surface microstructure of the specimen. The specimens were prepared for metallographic analysis by grinding them consecutively with 240, 600, and 1200-grit SiC paper, followed by polishing with 6 and 1 µm DIAMAT polycrystalline diamond cloths, finishing with 0.02 µm SIAMAT non-crystalline colloidal silica. The specimens were etched with Baker's reagent to expose the grain boundary formed by dynamic recovery or recrystallization.

2.3.2. Fracture Analysis

When the recycled specimens were broken, the breakage mode varied depending on the parameter setting. The fracture analysis was conducted using a JSM-7600F field emission scanning electron microscope (FESEM), JEOL, Akishima, Japan. The fracture samples were cut for testing into 1 cm × 1 cm × 1 cm units. The cause of breakage can

be determined from the breakage mode by examining the fracture surface of the broken material using FESEM. Fracture surface analysis is an effective tool for determining the cause of fractures.

2.3.3. Grain Analysis

Grain analysis was performed to measure the grain size of recycled specimens using atomic force microscopy (AFM) with an XE-100 from Park Systems, Suwon, South Korea. AFM is preferred due to its ability to produce a high vertical resolution for an aluminum specimen. This makes it feasible to precisely determine the grain size, which is related to the nanometric structure properties. The method used for AFM is a watershed with a filter level of three. The grain size was measured via an auto-statistic count.

2.3.4. Microhardness Test

The Vickers microhardness test was chosen to measure the hardness of the recycled specimens using small, applied loads. A Vickers microhardness tester, Shimadzu, Kyoto, Japan was used in this study. Testing was performed by pressing an indenter into the surface metal under a controlled force of 980.7 mN ($HV_{0.1}$) for 10 s, followed by removing the indenter and measuring the indentation size. A minimum of three indentations were made into each tested specimen.

2.3.5. Density Measurement

The density of the material was obtained using the Archimedean method by weighing small pieces cut from the specimens, first in the air and then in water. The density of the specimen was measured using a density balance (HR-250A, A&D, Seoul, Korea).

3. Results and Discussion

Table 4 represents the response data for the DR-HPF process with different parameters of holding time and temperature. As part of this study, the data included ultimate tensile strength (UTS), elongation to failure (ETF), density, and microhardness. This data was then grouped into mechanical properties and surface integrity.

Table 4. Data responses at different operating temperatures and holding times.

Sample Designation	Ultimate Tensile Test (UTS)	Elongation to Failure (ETF)	Microhardness	Density
	(MPa)	(%)	(HV)	(g/cm^3)
S1	17.02	0.53	45.79	1.645
S2	26.48	0.79	50.89	1.709
S3	43.48	0.87	51.89	2.290
S4	63.19	0.64	53.49	2.608
S5	77.85	1.05	55.97	2.699
S6	113.08	1.28	59.12	2.726
S7	185.89	2.30	61.58	2.755
S8	218.87	4.63	63.74	2.783
S9	245.62	6.91	69.02	2.795

3.1. Mechanical Properties

As shown in Figures 4 and 5, it was found that the UTS and ETF increased as the temperature and duration rose. The mechanical properties of aluminum alloys are dependent on the control of the temperature and time during processing [69]. The HPF process requires a high temperature that does not exceed the melting point for long enough for the phase containing copper and magnesium to completely dissolve, resulting in a virtually homogenous solid solution [32].

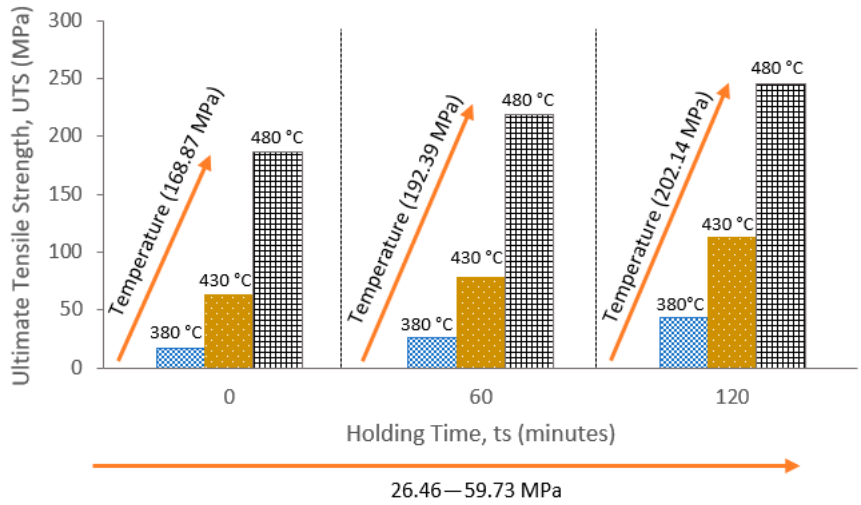

Figure 4. Ultimate tensile strength results at different working temperatures and duration.

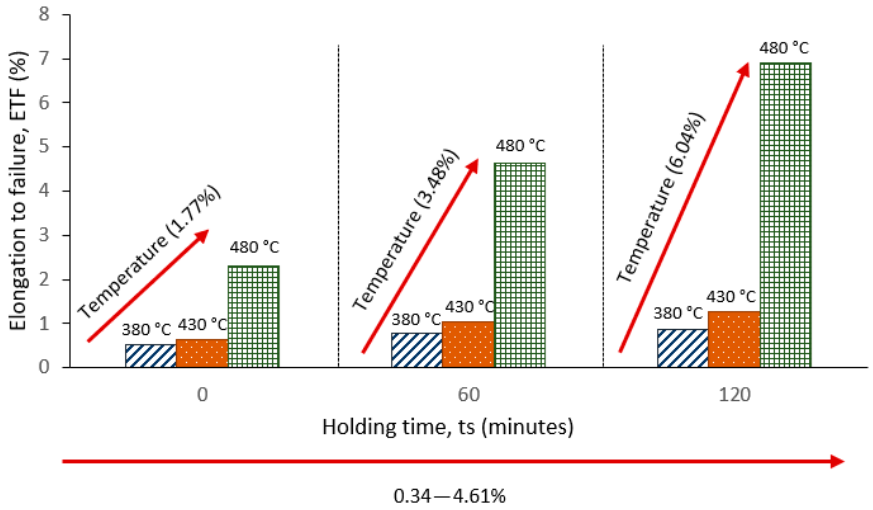

Figure 5. Elongation to failure results at different working temperatures and duration.

As seen in Figure 4, the inclination trend for UTS, depicted at a maximum duration of 120 min from 43.48 MPa (380 °C), surged up to 245.62 MPa (480 °C). At zero holding time, the UTS rose with increasing working temperatures, ranging from 17.02 MPa (380 °C) to 185.89 MPa (480 °C). The operating temperature has a substantial impact on the HPF process by demonstrating that, at a constant holding time, increasing the operating temperature from 380 °C to 480 °C increased the UTS value from 168.87 MPa to 202.14 MPa. In brief, the working temperature has the greatest influence in terms of enhancing the mechanical properties. Stress in a deformation process has a significant effect on forgeability [70]. The forgeability of metals increases with rising temperature as the grain size decreases, resulting in excellent tensile strength. Besides this, the solubility increases with temperature; therefore, working at a lower temperature will result in poorer properties [71]. Moreover, solid solution strengthening is likely to have a significant influence at high temperatures [32]. According to Sajadifar, the optimal temperature parameter for AA7075 aluminum alloy is 480 °C. The formation of detrimental intermetallic particles occurred when the temperature exceeded 480 °C [72]. Meng agreed that the increase in UTS was a result of the increase in heating temperature, stating that solute atoms were dissolved in the aluminum matrix during solutionizing and remained in a metastable state [69]. A similar trend has been observed when comparing the influence of holding time to UTS. At the temperature of 380 °C, the UTS value climbed from 17.20 MPa (0 min) to 43.48 MPa

(120 min). At a maximum temperature of 480 °C, the UTS value rises from 185.89 (0 min) to 245.62 (120 min).

As shown in Figure 5, the ETF exhibited a linear trend with increasing temperature, which is very similar to the UTS trend. At the maximum holding time (120 min), the ETF value for 380 °C was 0.87% and elevated up to 6.91 at 480 °C. At zero holding time, the ETF values rose with rising temperature from 0.53% (380 °C) to 2.30% (480 °C). The operating temperature showed a substantial influence on the HPF process by showing that the value of ETF rose from 1.77% to 6.04% when the temperature went from 380 °C to 480 °C at a constant holding time. Meanwhile, at the minimum temperature of 380 °C, the value of ETF went up from 0.53% (0 min) to 0.87% (120 min), while at the maximum operating temperature of 480 °C, the ETF value went up from 2.30% (0 min) to 6.91% (120 min).

By increasing the temperature from 380 to 480 °C at a maximum holding time of 120 min, the UTS grew by 82.3% and the ETF climbed by 87.41%. Meanwhile, when studying the effect of holding time from 0 to 120 min at the maximum working temperature of 480 °C, the UTS increased by 24.32% and ETF grew by 66.71%. Therefore, the operating temperature was the most influential factor in increasing the ETF and UTS. On the other hand, the UTS value increased from 17.02 MPa to 245.62 MPa when comparing the minimum-maximum parameter. The maximum parameter (480 °C/120 min) of the recycled sample shows a 7.17% increase over the theoretical AA7075-O value. The increase in UTS value clarifies the possibility of the HPF process being used as a meltless process.

3.2. Surface Integrity

3.2.1. Microstructural Analysis

Figure 6 and Table 5 show the microstructure and the grain size at the minimum S1 (380 °C/0 min) and maximum S9 (480 °C/120 min) parameters of the recycled AA7075 specimen, respectively. The images of the specimens were magnified at 50×. The images show the grain, grain boundary, and pores.

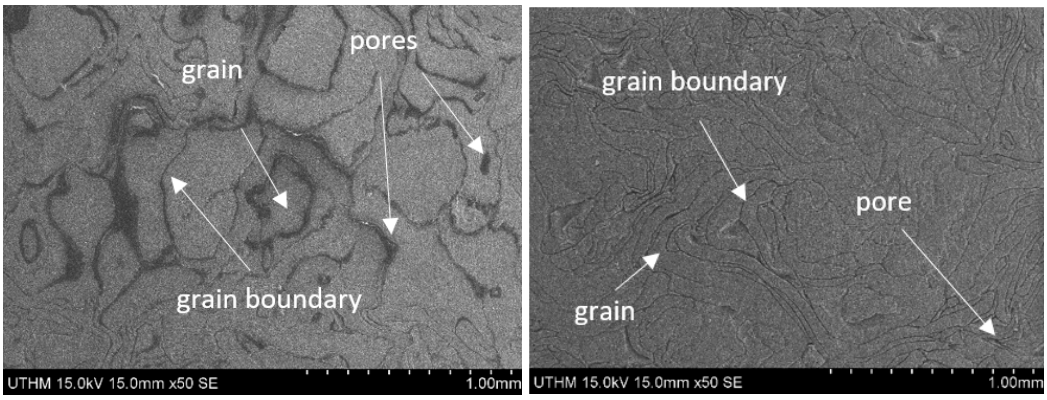

(**a**) (**b**)

Figure 6. Minimum and maximum parameters of the microstructure at 50× magnification for samples (**a**) S1 (380 °C/0 min) and (**b**) S9 (480 °C/120 min).

Table 5. Grain size for minimum and maximum hot-press forging parameters.

Sample Designation	Operating Temperature (°C)	Holding Time (Minutes)	Grain Size (μm)
S1	380	0	0.435
S2	380	120	0.212

S1 (380 °C/0 min) has a grain size of 0.435 μm, while S9 (480 °C/120 min) has a grain size of 0.212 μm, which is smaller than S1. The porosity of the microstructure can be clearly seen at the minimal parameter in Figure 6a, indicating that at this lowest temperature and

holding time, the chip is merely interlocking, rather than becoming consolidated with each other. The grain size appeared to be coarser as a result of the temperature being below recrystallization temperature [58].

On the contrary, when the temperature and holding time increase, the grain size decreased from 0.435 µm to 0.212 µm by 51.25%. As can be seen, increasing the working temperature and duration time resulted in a decrease in the void size between the aluminum chips. Furthermore, the crystalline size increased with increasing temperature and time [55]. The grain of the maximum parameter in Figure 6b became finer (0.212 µm) and with less porosity, due to the temperature above the recrystallization. This can be explained by the fact that, upon recrystallization, the structure entered the second phase of precipitation [56]. Attaining precipitation is accomplished by heating the aluminum alloy below the solidus line for a sufficient amount of time and temperature [58]. During this process, the atoms will diffuse to form fine precipitation [73]. These fine precipitates behave as a barrier to dislocation movement, increasing the initial strength [69].

The results from the tensile test show that grain size affects the mechanical properties. At the maximum working temperature and time, it can be seen that UTS and ETF had the highest values of 245.62 MPa and 6.91%, respectively, with a small grain size (0.212 µm) and less porosity in the microstructure.

3.2.2. Fracture Surface Analysis

Figure 7 shows an observation of the effect of minimum (380 °C/0 min) and maximum (480 °C/120 min) parameters on the fractured surface. When the metallic aluminum is broken, the breakage will vary, depending on the parameter setting of the HPF process. Figure 7a–c represents the fractured surfaces at minimum parameters, while Figure 7d–f represents the fractured surfaces at maximum parameters at different magnifications. At the minimum parameter, the fractured surface is revealed as shallow and flat, with no dimples at all. The image shows that fracture occurs along the crystallographic plane, known as the cleavage plane, with no plastic deformation where the normal stress is maximized [32]. At high magnification, as seen in Figure 7c, these flat areas exhibit fine cups and ridges. The metallic bonding between chips is also not fully formed, as a result of insufficient temperature and holding time. Low temperature leads to little or no oxidation and precision dimensioning, but it increases flow stress and decreases ductility, which promotes cracking [70]. This supports the result of the ETF value, which is as low as 0.53%.

At the maximum parameter, many microvoids and dimples can be seen, indicating the ductile fracture mode. The presence of deep and large dimples in Figure 7f indicates that the specimen has a high fluent strain. The maximum parameter has the highest ETF value, which is 6.92%. The higher temperature results in low stress and more ductility. The higher temperatures enhance ductility, allowing for greater plastic deformation [74].

3.2.3. Density and Microhardness Analysis

Figure 8 represent the overall density graph and microhardness graph at different parameters. As seen in Figure 8, the density and microhardness values increased with the increasing operating temperature and time. The minimum and maximum values of microhardness are 45.79 HV and 69.02 HV, respectively. Meanwhile, the minimum and maximum values of density were 1.645 g/cm^3 and 2.795 g/cm^3, respectively.

By increasing the temperature from 380 °C to 480 °C at the maximum holding time (120 min), the microhardness increased by 24.83% and the density increased by 18.04%. As the holding time increased from 0 to 120 min at maximum operating temperature, the microhardness increased by 10.78%, and the density increased by 1.43%. In short, the operating temperature yielded a higher percentage than the holding time. It can be concluded that the most influential factor for increasing microhardness and density is operating temperature. At the minimum and maximum holding times, the percentage of microhardness increased by 33.66%, while the density value increased by 41.14%. Insufficient working temperatures and holding times produce large gaps between the metal chips, hence decreasing

the material's density. Meanwhile, a fine grain size enhanced the microhardness of the aluminum alloy [75]. The highest value of the microstructure has a small amount of pore formation [76]. Therefore, increased grain boundaries, decreased grain size and porosity in the microstructure, and increased density led to a greater microhardness value [77].

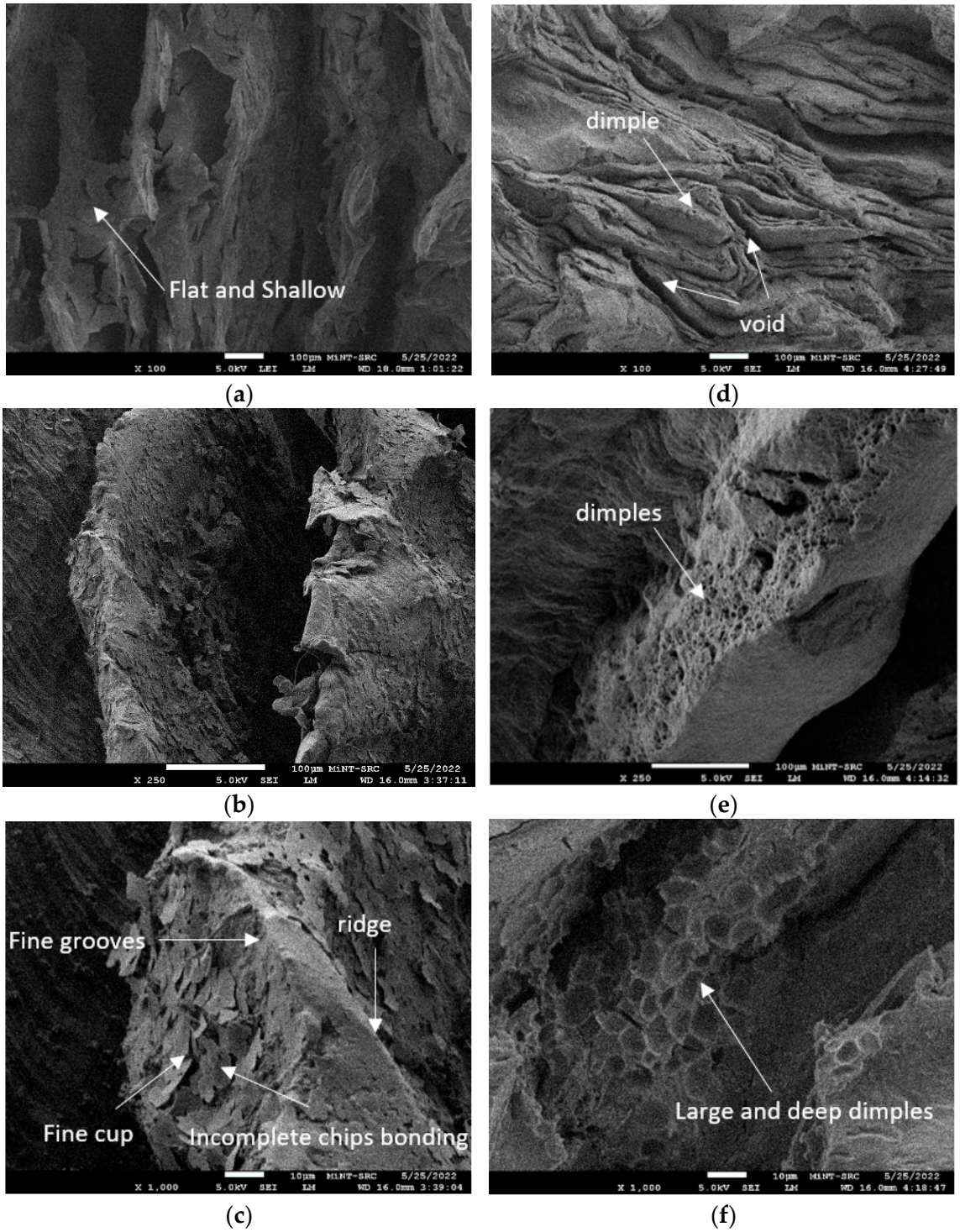

Figure 7. FESEM micrographs for surface fracture at minimum–maximum parameters: (**a**) an overview of the S1 fracture surface at 100×, (**b**) the periphery coarse topology of S1 at 250×, (**c**) equiaxed dimples of S1 at 1000×, (**d**) an overview of the S9 fracture surface at 100× (**e**) the periphery coarse topology of S9 at 250×, (**f**) the equiaxed dimples of S9 at 1000×.

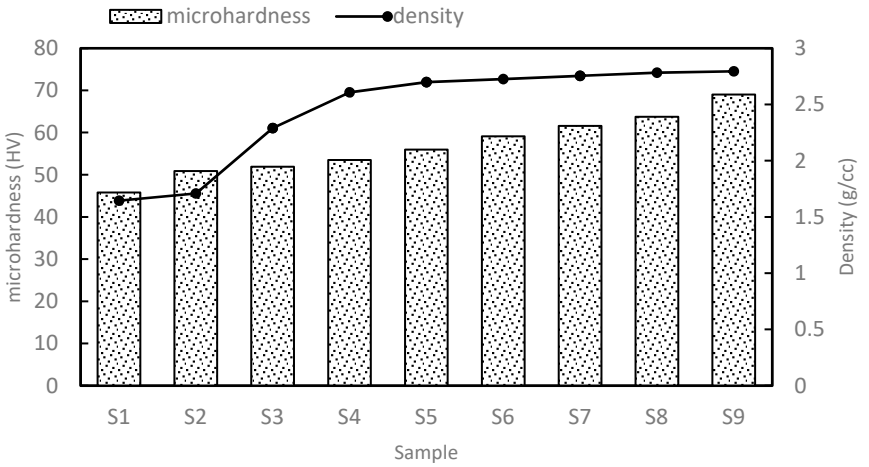

Figure 8. Microhardness and density graph at different temperatures and holding times.

4. Conclusions

The direct recycling of AA7075 aluminum alloys by employing the HPF process has a significant influence on the material's surface integrity and mechanical properties. The following is a succinct summary of the findings:

- The ETF value shows a linear trend with increasing temperature that is quite similar to the UTS trend. From the minimum (380 °C/0 min) to the maximum (480 °C/120 min) parameters, the UTS value increased by 93.07% and the ETF value increased by 92.33%.
- Increasing the operating temperature and time resulted in a decrease in the grain by 51.26% and in void size between the aluminum chips. At the maximum working temperature and time, it can be seen that UTS and ETF had the highest values of 245.62 MPa and 6.91%, respectively, with a small grain size (0.212 μm) and less porosity in the microstructure.
- At the minimum parameter, the fractured surface was revealed as shallow and flat, with no dimples at all. Meanwhile, at the maximum parameter, many microvoids and dimples can be seen, indicating the ductile fracture mode.
- From the minimum to maximum holding time, the percentage of microhardness increased by 33.66% and the density value increased by 41.14%.
- The most influential factor for increasing UTS, ETF, microhardness, and density is the operating temperature. The operating temperature contributes to a higher increment percentage result than the holding time.
- An increase in UTF and ETF values causes an increase in grain boundaries with the decrease in grain size, porosity in microstructure, and increased density, leading to a greater microhardness value.

Author Contributions: Conceptualization, N.E.R. and N.K.Y.; methodology, N.E.R., N.K.Y. and S.A.-A.; validation, N.E.R.; formal analysis, N.E.R.; investigation, N.E.R., N.K.Y., M.A.L., S.A.-A. and S.S.; resources, N.K.Y., M.A.L. and S.S.; data curation, N.E.R., S.A.-A. and I.S.T.T.; writing—original draft preparation, N.E.R.; writing—review and editing, W.Z. and N.K.Y.; visualization, N.E.R. and W.Z.; supervision, N.K.Y. and M.A.L.; project administration, N.K.Y.; funding acquisition, N.K.Y. All authors have read and agreed to the published version of the manuscript.

Funding: This research was funded by the Ministry of Higher Education (MOHE), Malaysia, which funded this project through the Fundamental Research Grant Schemes (FRGS/1/2019/TK09/UTHM/03/1) and monetary assistance by Universiti Tun Hussein Onn Malaysia and the UTHM Publisher's Office via the Publication Fund E15216.

Institutional Review Board Statement: Not applicable.

Informed Consent Statement: Not applicable.

Data Availability Statement: Not applicable.

Acknowledgments: The authors would like to express their deepest appreciation to the Ministry of Higher Education (MOHE), Malaysia for funding this project through the Fundamental Research Grant Schemes. Communication of this research is made possible through monetary assistance by Universiti Tun Hussein Onn Malaysia and the UTHM Publisher's Office via the Publication Fund E15216. Additional support in terms of facilities was also provided by Sustainable Manufacturing and Recycling Technology, Advanced Manufacturing and Material Center (SMART-AMMC), Universiti Tun Hussein Onn Malaysia (UTHM).

Conflicts of Interest: The authors declare no conflict of interest.

References

1. Ingarao, G.; Priarone, P.C.; Deng, Y.; Paraskevas, D. Environmental modelling of aluminium based components manufacturing routes: Additive manufacturing versus machining versus forming. *J. Clean. Prod.* **2018**, *176*, 261–275. [CrossRef]
2. Latif, A.; Ingarao, G.; Fratini, L. Multi-material based functionally graded billets manufacturing through friction stir consolidation of aluminium alloys chips CIRP Annals—Manufacturing Technology friction stir consolidation of aluminium alloys chips. *CIRP Ann.-Manuf. Technol.* **2022**, *71*, 261–264. [CrossRef]
3. Brough, D.; Jouhara, H. The aluminium industry: A review on state-of-the-art technologies, environmental impacts and possibilities for waste heat recovery. *Int. J. Thermofluids* **2020**, *2*, 100007. [CrossRef]
4. Priarone, P.C.; Ingarao, G.; Settineri, L.; Di, R. On the impact of recycling strategies on energy demand and CO_2 emissions when manufacturing Al-based components. *Procedia CIRP* **2016**, *48*, 194–199. [CrossRef]
5. Ingarao, G. Manufacturing strategies for efficiency in energy and resources use: The role of metal shaping processes. *J. Clean. Prod.* **2017**, *142*, 2872–2886. [CrossRef]
6. Joshi, T.C.; Prakash, U.; Dabhade, V.V. Microstructural development during hot forging of Al 7075 powder. *J. Alloys Compd.* **2015**, *639*, 123–130. [CrossRef]
7. Zhou, W.; Shao, Z.; Yu, J.; Lin, J. Advances and Trends in Forming Curved Extrusion Profiles. *Materials* **2021**, *14*, 1603. [CrossRef]
8. Zhou, W.; Lin, J.; Dean, T.A.; Wang, L. Analysis and modelling of a novel process for extruding curved metal alloy profiles. *Int. J. Mech. Sci.* **2018**, *138–139*, 524–536. [CrossRef]
9. Bulei, C.; Stojanovic, B.; Utu, D. Developments of discontinuously reinforced aluminium matrix composites: Solving the needs for the matrix Developments of discontinuously reinforced aluminium matrix composites: Solving the needs for the matrix. *J. Phys. Conf. Ser.* **2022**, *2022*, 012029. [CrossRef]
10. Kazemi-navaee, A.; Jamaati, R.; Aval, H.J. Asymmetric cold rolling of AA7075 alloy: The evolution of microstructure, crystallographic texture, and mechanical properties. *Mater. Sci. Eng. A* **2021**, *824*, 141801. [CrossRef]
11. Canakci, A.; Varol, T. Microstructure and properties of AA7075/Al-SiC composites fabricated using powder metallurgy and hot pressing. *Powder Technol.* **2014**, *268*, 72–79. [CrossRef]
12. Gancarczyk, K.; Nowotnik, A.; Boczkal, G. Microstructure and Properties of As-Cast and Heat-Treated 2017A Aluminium Alloy Obtained from Scrap Recycling. *Materials* **2021**, *14*, 89.
13. Dzurňák, R.; Augustín Varga, J.K.; Jablonský, G.; Lukáč, L. Influence of Burner Nozzle Parameters Analysis on the Aluminium Melting Process. *Appl. Sci.* **2019**, *9*, 1614. [CrossRef]
14. Ho, C.S.; Mohd Nor, M.K.; Ma'at, N.; Alaric Sim, K.Y.; Ibrahim, M.N.; Jamian, S.; Lajis, M.A.; Yusuf, N.K. Damage Initiation and Evolution Analysis of Hot Extruded Recycled Aluminium Alloys (AA6061). *Mater. Sci. Eng.* **2020**, *824*, 012017. [CrossRef]
15. Ingarao, G.; Zaheer, O.; Fratini, L. Manufacturing processes as material and energy ef fi ciency strategies enablers: The case of Single Point Incremental Forming to reshape end-of-life metal components. *CIRP J. Manuf. Sci. Technol.* **2021**, *32*, 145–153. [CrossRef]
16. Wan, B.; Chen, W.; Lu, T.; Liu, F.; Jiang, Z. Review of solid state recycling of aluminum chips. *Resour. Conserv. Recycl.* **2017**, *125*, 37–47. [CrossRef]
17. Söderholm, P.; Ekvall, T. Metal markets and recycling policies: Impacts and challenges. *Miner. Econ.* **2019**, *33*, 257–272. [CrossRef]
18. Dwivedi, S.P.; Sharma, P. Utilization of waste spent alumina catalyst and agro-waste rice husk ash as reinforcement materials with scrap aluminium alloy wheel matrix. *J. Process Mech. Eng.* **2020**, *234*, 543–552. [CrossRef]
19. Yasinskiy, A.; Padamata, S.K.; Moiseenko, I.; Stopic, S.; Feldhaus, D.; Friedrich, B.; Polyakov, P. Aluminium Recycling in Single- and Multiple-Capillary Laboratory Electrolysis Cells. *Metals* **2021**, *11*, 1053. [CrossRef]
20. Rivera, T.; Flores, A. A-242 Aluminium Alloy Foams Manufacture from the recycling of beverage cans. *Metals* **2019**, *9*, 92. [CrossRef]
21. Wong, D.S.; Lavoie, P. Aluminum: Recycling and Environmental Footprint. *JOM* **2019**, *71*, 2926–2927. [CrossRef]
22. Paraskevas, D.; Kellens, K.; Dewulf, W.; Duflou, J.R. Resource Efficiency in Manufacturing: Identifying Low Impact Paths. In Proceedings of the 10th Global Conference on Sustainable Manufacturing (GCSM 2012), Istanbul, Turkey, 31 October–2 November 2012; pp. 271–276.
23. Ingarao, G.; Baffari, D.; Bracquene, E.; Fratini, L.; Duflou, J. Energy demand reduction of aluminum alloys recycling through friction stir extrusion processes implementation. *Procedia Manuf.* **2019**, *33*, 632–638. [CrossRef]

24. Buffa, G.; Baffari, D.; Ingarao, G.; Fratini, L. Uncovering Technological and Environmental Potentials of Aluminum Alloy Scraps Recycling Through Friction Stir Consolidation. *Int. J. Precis. Eng. Manuf.-Green Technol.* **2020**, *7*, 955–964. [CrossRef]
25. Rady, M.H.; Mustapa, M.S.; Wagiman, A.; Shamsudin, S.; Lajis, M.A.; Al Alimi, S.; Mansor, M.N.; Harimon, M.A. Effect of the heat treatment on mechanical and physical properties of direct recycled aluminium alloy (AA6061). *Int. J. Integr. Eng.* **2020**, *12*, 82–89. [CrossRef]
26. Paraskevas, D.; Kellens, K.; Dewulf, W.; Du, J.R. Environmental modelling of aluminium recycling: A Life Cycle Assessment tool for sustainable metal management. *J. Clean. Prod.* **2014**, *105*, 357–370. [CrossRef]
27. Baffari, D.; Reynolds, A.P.; Masnata, A.; Fratini, L.; Ingarao, G. Friction stir extrusion to recycle aluminum alloys scraps: Energy efficiency characterization. *J. Manuf. Process.* **2019**, *43*, 63–69. [CrossRef]
28. Shen, H.; Liu, B.; Ekberg, C.; Zhang, S. Harmless disposal and resource utilization for secondary aluminum dross: A review. *Sci. Total Environ.* **2021**, *760*, 143968. [CrossRef] [PubMed]
29. Hatayama, H.; Daigo, I.; Matsuno, Y.; Adachi, Y. Evolution of aluminum recycling initiated by the introduction of next-generation vehicles and scrap sorting technology. *Resour. Conserv. Recycl.* **2012**, *66*, 8–14. [CrossRef]
30. Lajis, M.A.; Yusuf, N.K.; Ahmad, A. Life cycle assessment on the effects of parameter setting in direct recycling hot press forging of aluminum. *Mater. Sci. Forum* **2018**, *923 MSF*, 143–148. [CrossRef]
31. Koch, A.; Bonhage, M.; Teschke, M.; Luecker, L.; Behrens, B.; Walther, F. Electrical resistance-based fatigue assessment and capability prediction of extrudates from recycled field-assisted sintered EN AW-6082 aluminium chips. *Mater. Charact.* **2020**, *169*, 110644. [CrossRef]
32. Yusuf, N.K.; Lajis, M.A.; Ahmad, A. Hot press as a sustainable direct recycling technique of aluminium: Mechanical properties and surface integrity. *Materials* **2017**, *10*, 902. [CrossRef] [PubMed]
33. Duflou, J.R.; Tekkaya, A.E.; Haase, M.; Welo, T.; Vanmeensel, K.; Kellens, K.; Dewulf, W.; Paraskevas, D. Environmental assessment of solid state recycling routes for aluminium alloys: Can solid state processes significantly reduce the environmental impact of aluminium recycling? *CIRP Ann.-Manuf. Technol.* **2015**, *64*, 37–40. [CrossRef]
34. Wagiman, A.; Mustapa, M.S.; Asmawi, R.; Shamsudin, S.; Lajis, M.A.; Mutoh, Y. A review on direct hot extrusion technique in recycling of aluminium chips. *Int. J. Adv. Manuf. Technol.* **2020**, *106*, 641–653. [CrossRef]
35. Zhou, W.; Yu, J.; Lin, J.; Dean, T.A. Manufacturing a curved profile with fine grains and high strength by differential velocity sideways extrusion. *Int. J. Mach. Tools Manuf.* **2019**, *140*, 77–88. [CrossRef]
36. Zhou, W.; Yu, J.; Lu, X.; Lin, J.; Dean, T.A. A comparative study on deformation mechanisms, microstructures and mechanical properties of wide thin-ribbed sections formed by sideways and forward extrusion. *Int. J. Mach. Tools Manuf.* **2021**, *168*, 103771. [CrossRef]
37. Zhou, W.; Yu, J.; Lin, J.; Dean, T.A. Effects of die land length and geometry on curvature and effective strain of profiles produced by a novel sideways extrusion process. *J. Mater. Process. Tech.* **2020**, *282*, 116682. [CrossRef]
38. Al-Alimi, S.; Lajis, M.; Shamsudin, S.; Yusuf, N.K.; Altharan, Y.; Didane, D.H.; Saif, Y.; Sadeq, S.; Sabbar, H.M.; Msebawi, M.S. Effects of Preheating Temperature on Deformed AA6061 Aluminium Properties of Hot Equal Channel Angular Pressing (ECAP) by Using Deform-3D Software. *Arab. J. Sci. Eng.* **2022**, *47*, 1–9. [CrossRef]
39. Al Alimi, S.; Shamsudin, S.; Yusuf, N.K.; Lajis, M.A.; Zhou, W.; Didane, D.H.; Sadeq, S.; Saif, Y.; Wahib, A.; Harun, Z. Recycling Aluminium AA6061 Chips with Reinforced Boron Carbide (B4C) and Zirconia (ZrO_2) Particles via Hot Extrusion. *Metals* **2022**, *12*, 1329. [CrossRef]
40. Gronostajski, J.Z.; Kaczmar, J.W.; Marciniak, H.; Matuszak, A. Direct recycling of aluminium chips into extruded products. *J. Mater. Process. Technol.* **1997**, *64*, 149–156. [CrossRef]
41. Fogagnolo, J.B.; Ruiz-Navas, E.M.; Simón, M.A.; Martinez, M.A. Recycling of aluminium alloy and aluminium matrix composite chips by pressing and hot extrusion. *J. Mater. Process. Technol.* **2003**, *143–144*, 792–795. [CrossRef]
42. Haase, M.; Tekkaya, A.E. Cold extrusion of hot extruded aluminum chips. *J. Mater. Process. Technol.* **2015**, *217*, 356–367. [CrossRef]
43. Güley, V.; Güzel, A.; Jäger, A.; Ben Khalifa, N.; Tekkaya, A.E.; Misiolek, W.Z. Effect of die design on the welding quality during solid state recycling of AA6060 chips by hot extrusion. *Mater. Sci. Eng. A* **2013**, *574*, 163–175. [CrossRef]
44. Gronostajski, J.; Marciniak, H.; Matuszak, A. New methods of aluminium and aluminium-alloy chips recycling. *J. Mater. Process. Technol.* **2000**, *106*, 34–39. [CrossRef]
45. Tekkaya, A.E.; Schikorra, M.; Becker, D.; Biermann, D.; Hammer, N.; Pantke, K. Hot profile extrusion of AA-6060 aluminum chips. *J. Mater. Process. Technol.* **2008**, *9*, 3343–3350. [CrossRef]
46. Li, J.; Zhang, A.; Pan, H.; Ren, Y.; Zeng, Z.; Huang, Q. Effect of extrusion speed on microstructure and mechanical properties of the Mg-Ca binary alloy. *J. Magnes. Alloys* **2021**, *9*, 1297–1303. [CrossRef]
47. Rahim, S.N.A.; Lajis, M.A.; Tun, U.; Onn, H. Effect of extrusion speed and temperature on hot extrusion process of 6061 aluminum alloy chip. *ARPN J. Eng. Appl. Sci.* **2016**, *11*, 2272–2277.
48. Rahim, S.N.A.; Lajis, M.A.; Ariffin, S. A Review on Recycling Aluminum Chips by Hot Extrusion Process. *Procedia CIRP* **2015**, *26*, 761–766. [CrossRef]
49. Al-alimi, S.; Lajis, M.A.; Shamsudin, S.; Yusuf, N.K.; Chan, B.L.; Hissein, D.D.; Rady, M.H.; Msebawi, M.S.; Sabbar, H.M. Hot extrusion followed by a hot ecap consolidation combined technique in the production of boron carbide (b4c) reinforced with aluminium chips (aa6061) composite. *Mater. Technol.* **2021**, *55*, 347–354. [CrossRef]

50. Al-alimi, S.; Amri, M.; Shamsudin, S.; Kamilah, N. Development of Hot Equal Channel Angular Processing (ECAP) Consolidation Technique in the Production of Boron Carbide (B4C)-Reinforced Aluminium Development of Hot Equal Channel Angular Processing (ECAP) Consolidation Technique in the Production of Boron. *Int. J. Renew. Energy Dev.* **2021**, *10*, 607–621. [CrossRef]
51. Krolo, J.; Lela, B.; Dumanić, I. Statistical analysis of the combined ecap and heat treatment for recycling aluminum chips without remelting. *Metals* **2019**, *9*, 660. [CrossRef]
52. Khajouei-Nezhad, M.; Paydar, M.H.; Mokarizadeh Haghighi Shirazi, M.; Gubicza, J. Microstructure and Tensile Behavior of Al7075/Al Composites Consolidated from Machining Chips Using HPT: A Way of Solid-State Recycling. *Met. Mater. Int.* **2019**, *26*, 1881–1898. [CrossRef]
53. Kuzman, K.; Kacmarcik, L.; Pepelnjak, T.; Plancak, M.; Vilotic, D. Experimental consolidation of aluminium chips by cold compression. *J. Prod. Eng.* **2012**, *15*, 79–82.
54. Khamis, S.S.; Lajis, M.A.; Albert, R.A.O. A sustainable direct recycling of aluminum chip (AA6061) in hot press forging employing Response surface methodology. *Procedia CIRP* **2015**, *26*, 477–481. [CrossRef]
55. Ahmad, A.; Lajis, M.A.; Yusuf, N.K.; Ab Rahim, S.N. Statistical optimization by the response surface methodology of direct recycled aluminum-alumina metal matrix composite (MMC-AlR) employing the metal forming process. *Processes* **2020**, *8*, 805. [CrossRef]
56. Ahmad, A.; Lajis, M.A.; Yusuf, N.K.; Wagiman, A. Hot press forging as the direct recycling technique of aluminium—A review. *ARPN J. Eng. Appl. Sci.* **2016**, *11*, 2258–2265.
57. Yusuf, N.K.; Lajis, M.A.; Ahmad, A. Multiresponse optimization and environmental analysis in direct recycling hot press forging of aluminum AA6061. *Materials* **2019**, *12*, 1918. [CrossRef]
58. Yusuf, N.K.; Lajis, M.A.; Daud, M.I.; Noh, M.Z. Effect of operating temperature on direct recycling aluminium chips (AA6061) in hot press forging process. *Appl. Mech. Mater.* **2013**, *315*, 728–732. [CrossRef]
59. Yusuf, N.K. *Effect of Hot Press Forging Parameter and Life Cycle Assessment in Direct Recycling of AA6061 Aluminium*; Universiti Tun Hussein Onn Malaysia: Parit Raja, Malaysia, 2017.
60. ASM International Handbook Committee. *Forging of Aluminum Alloys*; ASM International Handbook Committee: Almere, The Netherlands, 2005; Volume 14A.
61. Huo, W.; Guo, M.; Hou, L.; Cui, H.; Sun, T.; Zhuang, L.; Zhang, J. Recrystallization behavior of high-strength AA 7075 alloy processed by new short-cycled thermo-mechanical processing. *Mater. Sci. Forum* **2014**, *794–796*, 1269–1274. [CrossRef]
62. Wang, L.; Yang, X.; Robson, J.D.; Sanders, R.E.; Liu, Q. Microstructural Evolution of Cold-Rolled AA7075 Sheet during Solution Treatment. *Materials* **2020**, *13*, 2734. [CrossRef]
63. Bakkiyaraj, M.; Palanisamy, P.; Pk, N. Effect of post-weld heat treatment on tensile strength and microstructure characteristics in dissimilar friction welded (AA6061—AA7075-T6) joints Effect of post-weld heat treatment on tensile strength and microstructure characteristics in dissimilar f. *Mater. Res. Express* **2020**, *6*, 1265c1. [CrossRef]
64. Sun, S.; Liu, P.; Hu, J.; Hong, C.; Qiao, X.; Liu, S.; Zhang, R.; Wu, C. Effect of solid solution plus double aging on microstructural characterization of 7075 Al alloys fabricated by selective laser melting (SLM). *Opt. Laser Technol.* **2019**, *114*, 158–163. [CrossRef]
65. Wang, X.; Pan, Q.; Liu, L.; Xiong, S.; Wang, W.; Lai, J.; Sun, Y.; Huang, Z. Characterization of hot extrusion and heat treatment on mechanical properties in a spray formed ultra-high strength Al-Zn-Mg-Cu alloy. *Mater. Charact.* **2018**, *144*, 131–140. [CrossRef]
66. Pankade, S.B.; Khedekar, D.S.; Gogte, C.L. The influence of heat treatments on electrical conductivity and corrosion performance of AA 7075-T6 aluminium alloy. *Procedia Manuf.* **2018**, *20*, 53–58. [CrossRef]
67. Lu, T.; Chen, W.; Xu, W.; Wang, P.; Mao, M.; Liu, Y.; Fu, Z. The effects of Cr particles addition on the aging behavior and mechanical properties of SiCp/7075Al composites. *Mater. Charact.* **2018**, *136*, 264–271. [CrossRef]
68. Yusuf, N.K.; Lajis, M.A.; Ahmad, A. Life Cycle Assessment on the Direct Recycling Aluminium Alloy AA6061 Chips and Metal Matrix Composite (MMC-AlR). *Int. J. Integr. Eng.* **2021**, *7*, 95–100.
69. Meng, C. Effect of Preheating Condition on Strength of AA6060 Aluminium Alloy for Extrusion. Ph.D. Thesis, Auckland University of Technology, Auckland, New Zealand, 2010.
70. ASM International Handbook Committee. *Forming and Forging*; ASM International Handbook Committee: Almere, The Netherlands, 2006; Volume 14.
71. Monteiro, V.M. Microstructural and mechanical study of aluminium alloys submitted to distinct soaking times during solution heat treatment. *Tecnol. Em Metal. Mater. E Min.* **2014**, *11*, 332–339. [CrossRef]
72. Sajadifar, S.V.; Moeini, G.; Scharifi, E.; Lauhoff, C.; Böhm, S.; Niendorf, T. On the Effect of Quenching on Postweld Heat Treatment of Friction-Stir-Welded Aluminum 7075 Alloy. *J. Mater. Eng. Perform.* **2019**, *28*, 5255–5265. [CrossRef]
73. Rashid, M. Mathematical Modeling and Optimization of Precipitation Hardening of Extrudable Aluminum Alloys. Ph.D. Thesis, King Fahd University of Petroleum and Minerals, Dhahran, Saudi Arabia, 1997.
74. Groover, M.P. *Fundamentals of Modern Manufacturing: Materials, Processes, and Systems*; John Wiley & Sons: Hoboken, NJ, USA, 2013; Volume 53, ISBN 9788578110796.
75. Ahmad, A.; Lajis, M.A.; Yusuf, N.K. On the role of processing parameters in Producing recycled aluminum AA6061 based metal matrix composite (MMC-AlR) prepared using hot press forging (HPF) process. *Materials* **2017**, *10*, 98. [CrossRef]

76. Kadir, M.I.A.; Mustapa, M.S.; Mahdi, A.S.; Kuddus, S.; Samsi, M.A. Evaluation of hardness strength and microstructures of recycled Al chip and powder AA6061 fabricated by cold compaction method. *IOP Conf. Ser. Mater. Sci. Eng.* **2017**, *166*, 012012. [CrossRef]
77. Kumar, M.; Kumar, A.; Ji, H.; Song, Q.; Liu, Z.; Cai, W.; Mia, M.; Khanna, N. Impact of layer rotation on micro-structure, grain size, surface integrity and mechanical behaviour of SLM Al-Si-10Mg alloy. *Integr. Med. Res.* **2020**, *9*, 9506–9522. [CrossRef]